Int. J. Electrochem. Sci., 15 **(2020)** 6343 – 6358, doi: 10.20964/2020.07.78

International Journal of
ELECTROCHEMICAL
SCIENCE
www.electrochemsci.org

Electrodeposition of Ni–Co / nano Al_2O_3 composite coating on low carbon steel and its characterization

M.M. Kamel [1], *Z. Abdel Hamid* [2], *S.M. Rashwan* [1], *I.S. Ibrahim* [3], *S.M. El–Sheikh* [2], *M.M. Mohamed* [4*]

[1] Department of Chemistry, Faculty of Science, Suez Canal University, Ismailia, 41522, Egypt.
[2] Central Metallurgical Research & Development Institute, CMRDI, Helwan, Cairo, Egypt.
[3] General Organization for Exports and Imports Control (GOEIC), Royal International Inspection Laboratories (RIIL), Sokhna Port, Suez, Egypt.
[4] Department of Chemistry of Sharourah's Faculty of Science and Art, Najran University, Saudi Arabia.
[*]E-mail: mmmohammad@nu.edu.sa

Received: 14 March 2020 / *Accepted:* 11 May 2020 / *Published:* 10 June 2020

Ni–Co / nano-Al_2O_3 composite coat was electrodeposited from environmentally friendly citrate tub. The electrodeposition was established from agitated solutions, containing disparate amounts of nano-Al_2O_3 particles. The addition of nano - Al_2O_3 to the plating solution decreases the polarization for Ni–Co alloy plating. The quantity of Al_2O_3 in the composite rises with concentration of Al_2O_3 in the coating solution, current density and decreasing temperature. Composites were examined by scanning electron microscopy (SEM), X-ray diffraction (XRD) and energy dispersive X – ray (EDX) techniques. The obtained composites were crystalline and had face-centered cubic (FCC) structure. The thickness of composite diminishes with increasing the amount of Al_2O_3 in the composite however, the microhardness increases. The resistance of Ni–Co / nano-Al_2O_3 composite against corrosion in 3.5 % salt water was tested by potentiodynamic polarization and electrochemical impedance spectroscopy (EIS). Ni–Co / nano-Al_2O_3 composites had a good corrosion resistance.

Keywords*:* electrodeposition; citrate bath; Ni–Co / nano-Al_2O_3; microhardness

1. INTRODUCTION

Electrodeposited metallic composites may be single metal or alloy. These composites are harder to be applied in severe environments, which are subjected to both chemical and mechanical wear attack. As a result, there was an exigent necessity to create novel classes of wear- and corrosion-resistant coating materials [1].

There is a growing demand to ameliorate Metal Matrix Composites coatings (MMCs). Advances in technology need materials with particular properties. In general, composites possess topnotch characteristics such as eminent hardness, acceptable resistance to corrosion at higher temperatures, surpass wear and oxidation resistances. In addition to electrical and magnetic properties, self-lubrication, tensile and breakage strength, high thermal stability, chemical and biological compatibility relative to conventional pure metal or metallic alloy composites [1–3].

Nano-particles show various specific physical & chemical properties due to quantum size and quantum tunnel effects. Nano-composites plating technique, in which nanoparticles are inserted into to metallic composites, to enhance their physical & mechanical properties, illustrates how nanotechnology can be utilized for plating of composites.

Composites can be obtained by a variety of techniques such as thermal spraying, plasma spraying, chemical vapor deposition (CVD), physical vapor deposition (PVD), electroless deposition and electrodeposition [4–6]. Among these techniques electrodeposition technique has proved itself to be a promising technique to produce metal matrix composites in a single step. It produces harder and smoother surfaces. This enhances bonding among codeposited molecules and metal and allows fine control for the coating thickness [7 & 8].

Electrodeposited MMCs fundamentally composed of elastic metal / alloy matrix in which another fine indissoluble inert phase with a diversified particle size, ranges from micrometric and sub-micrometric to nano-metric one, is distributed [9 &10]. The particle size has a pronounced effect on the properties of the coating. In chief, the properties of the coat were improved greatly as the particle size of codeposited particles decreases [11]. In the last few years, a variety of nano-sized particles ranging from 4 - 800 nanometers have been incorporated successfully into metallic composites. Currently, there is a growing trend to use particles less than 100 nanometers to obtain a new innovative of advanced materials [12 &13].

The particles that used in composites were categorized into 2 important categories: soft & hard particles. Soft particles act as self-lubricant substances to minify friction between sliding surfaces. On the other hand, hard particles such as SiO_2, Al_2O_3, SiC, and Si_3N_4 amend the mechanical properties and microhardness of deposited metals and alloys [14–17].

Ceramics in the form of oxides are inorganic compounds of metallic (Al, Ti, Cr) or metalloid (Si) elements with oxygen. They have the ability form a variety of composites with different metallic matrixes. They are utilized to increase the oxidation resistance, hardness and wear improvement over conventional composites. Several oxides such as alumina (Al_2O_3), silica (SiO_2), chromia (Cr_2O_3), ferric oxide (Fe_2O_3), zirconia (ZrO_2), ceria (CeO_2), titania (TiO_2), yttria (Y_2O_3), Dysprosium oxide (Dy_2O_3) and lanthana (La_2O_3) form different composites with various metallic matrixes [17– 24].

Alumina particles are one of the most studied ceramic materials [25-38]. It has many unique properties such as great chemical stability, utmost elastic modulus, large thermal stability, high hardness and corrosion resistance [25–27]. Moreover, it is an electrically nonconducting substance [28]. Wu and coworkers [26] prepared Ni–Co/Al_2O_3 composites using codeposition of alloys and Al_2O_3 from sulfamate tub. They studied the effect of plating conditions on the amount of Al_2O_3 particles in Ni–Co alloys. Chang and his team [29] deposited Ni–Co/Al_2O_3 composite coating using

pulse reverse current under ultrasonic conditions. The effect of ultrasonic power on composition, appearance, microhardness microstructure & residual macrostress of composite coating was studied.

The given work aims to electrodeposit Ni–Co / nano-Al_2O_3 composites coating at low carbon steel cathode. The deposition was established from conventional citrate bath by electrodeposition technique. The study was carried out under different experimental conditions and comprises the evaluation of microstructure of the prepared composites by (SEM), (EDX) & (XRD) techniques. The corrosion resistance of composites is tested in 3.5 % salt water by potentiodynamic measurements and impedance technique.

2. EXPERIMENTAL

2.1. Electrodeposition procedure

Electrodeposition was established from solutions contain 0.08 M nickel sulphate e, 0.12 M cobalt sulphate, 0.2 M anhydrous sodium sulphate, 0.3 M tri – sodium citrate and different amounts of nano-sized Al_2O_3 powder with average size of 16.4 nm. Agglomeration of Al_2O_3 was minified by ultrasonic dispersion for 20 minutes. The pH was measured using digital Fisher pH-meter.

The experimental setup was mentioned formerly [39]. It composed of a Perspex trough, in the form of rectangle, equipped with a sheet of low carbon steel cathode and a stainless steel (type – 304) sheet anode. Every sheet had a total area of 9 cm^2. The working sheet was burnished mechanically with progressively fine grades of emery papers, cleaned with bi-distilled water, rinsed with acetone and weighed. The plating was completed from agitated solutions. The deposition time was 20 minutes, after which the coated steel was washed with bi-distilled water, dried & weighed. The alloy composition was ascertained by atomic absorption spectrophotometer (type Solaar S4). It was found that the proportion of Al_2O_3 nano particles in the composites ranging from 2.5 to 4.4%.

2.2. Potentiodynamic polarization measurements

Corrosion of composite coating in 3.5 wt. % salt water was examined by potentiodynamic polarization. This is carried out by the aid of an electrochemical analyzer (Iviumstat Electrochemical Interface) supplied by IVIUM technologies. The electrochemical analyzer is linked to a personal computer for potential control and data acquisition and a classical three-electrode cell with a steel working electrode of exposed area of 1 cm^2. All potentials measured referred to saturated calomel electrode (SCE). Pt gauze acted at counter electrode. Before starting run, steel electrode was immersed in the test solution for 30 minutes to achieve steady state. The potentials were scanned from −0.5V below OCP to a final potential of +0.5 V, at a sweep rate of 1 mV s^{-1}. Three experiments were made for each sample to ensure reliability. The corrosion potential (E_{corr}) and corrosion current density (I_{corr}) obtained from the intersection of the cathodic and anodic polarization curves constructed by Tafel extrapolation methods are listed in Tables 3. The corrosion current density (i_{corr}) was measured using the following equation:

$$I_{corr} = B / R_p \qquad (1)$$

Where: R_p is the polarization resistance & B is the Stern–Geary constant, calculated by the following equation:

$$B = \frac{\beta a.\beta c}{2.303(\beta a + \beta c)} \quad (2)$$

Where: β_a and β_c are the anodic and cathodic Tafel slopes, respectively.

The corrosion current density (I_{corr}) can be converted to corrosion rates (mm/year) based on the following Faraday's law:

$$\text{Corrosion rate} = 3.15 \times 10^5 \times \left(\frac{M}{nFd}\right) \times I_{corr} \quad (3)$$

Where M *is* atomic mass, n is the number of electrons involved in the corrosion reaction in mole (n = 2), F is Faraday's constant in coulombs/mole (F = 96500), and d is the density of alloy in g/cm^3 (d = 9.55).

2.3. Electrochemical impedance spectroscopy measurements

(EIS) measurements were carried out in the frequency range of 60 kHz - 10 MHz with a 5 mV sine wave as excitation signal. The corrosive medium was a solution of 3.5 wt. % salt water. The experiments were carried out at a fixed temperature (±1 °C). For investigational data, the parameters as a proportional factor (Y_o), phase shift (n), R_s, and R_{ct} were evaluated using the ZSimpWin program. The fitted impedance parameters are given in Table 4. The CPE type impedance, Z_{CPE}, was calculated from the subsequent equation:

$$Z_{CPE} = \frac{1}{Y_o(j\omega)^n} \quad (4)$$

Where the exponent n is the phase shift; provides information about the degree of non- ideality in capacitive behavior, $J^2 = -1$, $\omega = 2\pi f$. For $n = 0$, Z_{CPE} represents a resistance with $R = {Y_o}^{-1}$, for $n = 1$ a capacitance with $C = Y_o$, for $n = 0.5$ a Warburg impedance with $W = Y_o$ and for $n = -1$ an inductive with $L = {Y_o}^{-1}$.

2.4. Coating characterization

The morphology of composites was checked by (SEM) (QUATNTA FEG 250) engaged with energy dispersive spectrometer (EDX – FEI – QUATNTA FEG 250). The latter was utilized to identify the components of the composites. Microstructure of the composite coating was analyzed by X – ray diffractometer (X`pert Pro P analytical operated at 45 KV & 40 mA with Cu-Kα radiation λ = 0.154 nm). The thickness of the composites was determined by coating thickness gauge (model TT210). The thickness of the composites ranged from 6.5 to 11 μm. Microhardness was measured by microhardness tester with a load force of 100 g for 5 seconds. The microhardness was found to be ranged from 140 to 330 Hv.

3. RESULTS AND DISCUSSION

3.1. Cathodic polarization measurements

To expound the influence of nano - sized Al_2O_3 inert particles on the electrodeposition process of Ni–Co alloy, cathodic polarization experiments were carried out [40]. Polarization methods involve changing the working electrode potential and measured the corresponding current that is produced [41].

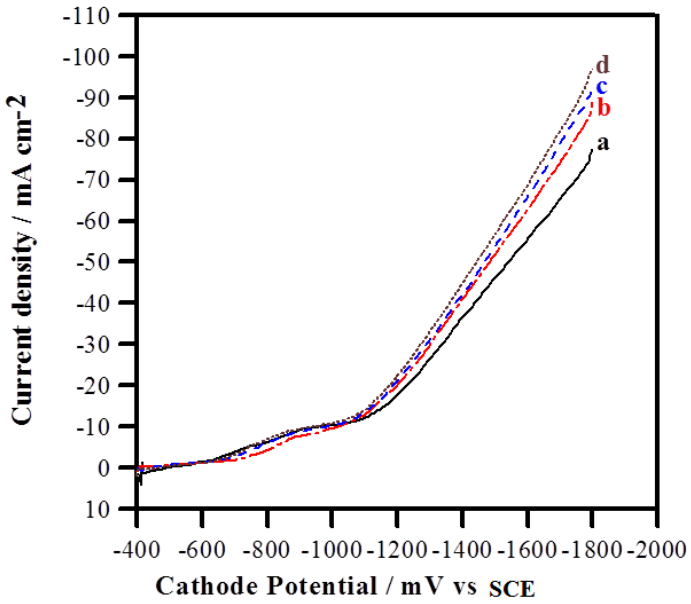

Figure 1. Cathodic polarization curves for Ni-Co / Al_2O_3 composite on steel at pH = 10, temperature = 25 °C and stirring speed = 500 rpm from solutions with 0.08 M $NiSO_4$. $6H_2O$, 0.12 M $CoSO_4.7H_2O$, 0.3 M $Na_3C_6H_5O_7.2H_2O$, 0.2 M Na_2SO_4 and different concentrations of nano sized Al_2O_3: (a) 0, (b) 1, (c) 2 and (d) 4 g/l. Scan rate = 20 mV/s.

The impact of concentration of nano-sized Al_2O_3 particles in the coating tub, upon the cathodic polarization of Ni–Co alloy is illustrated in figure (1). Increasing the content of Al_2O_3 particles in the plating tub reduces polarization for Ni–Co alloy plating. Al_2O_3 particles facilitate alloy deposition [42]. This behavior was reported for conducting particles such as Cr particles and semi-conducting particles like SiC [43]. The noble shift for deposition potential of Ni–Co alloy ascribed to improvement in the rate of transfer of depositing ions by Al_2O_3 nano particles. This increases the metal nuclei on the steel sheet and thusly encouraging its deposition [44]. In addition, Al_2O_3 nanoparticles can facilitate the adsorption of the alloying ions and hence increment the current density [45& 46].

3.2. Composition of composites

The content of particles and their dispersion in electrodeposited composites mainly depend on numerous parameters such as concentration and size of inert particles, the utilized current density, and

the deposition temperature, pH of the bath, agitation and deposition time [47]. The effects of some variables on the electrodeposition process are shown in Figs (2 – 4).

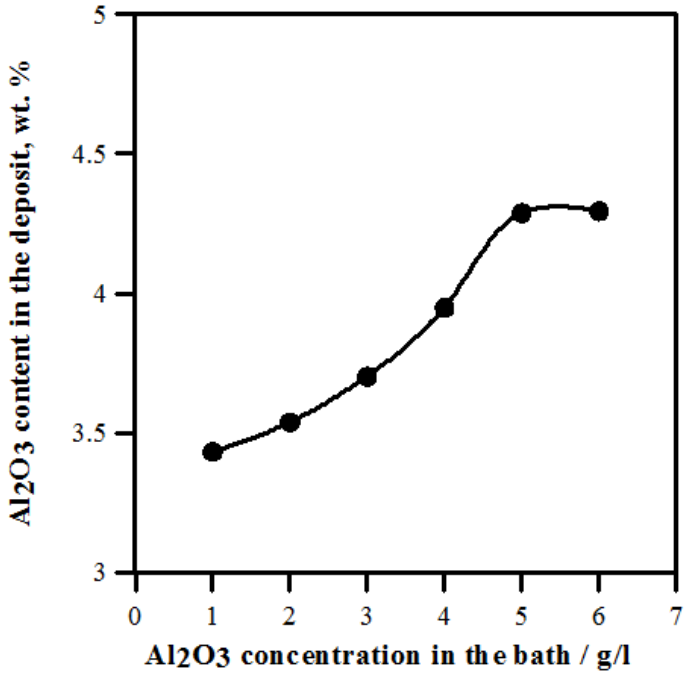

Figure 2. The impact of concentration of nano Al_2O_3 particles on the composition of Ni-Co / Al_2O_3 composite on steel from a bath with 0.08 M $NiSO_4.6H_2O$, 0.12 M $CoSO_4.7H_2O$, 0.3 M $Na_3C_6H_5O_7.2H_2O$, 0.2 M Na_2SO_4 and different concentrations of nano Al_2O_3 at time = 20 min., pH = 10, current density = 55.55 mA cm^{-2}, temperature = 25 ˚C and stirring speed = 500 rpm.

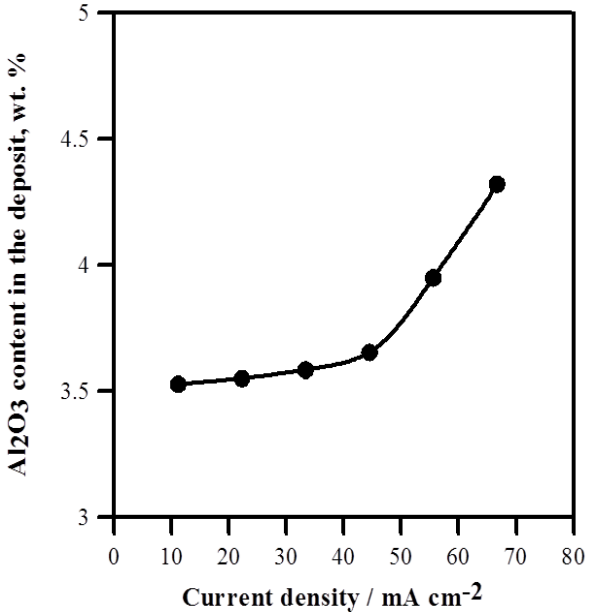

Figure 3. The impact of current density on the composition of Ni-Co / Al_2O_3 composite on steel from a bath with 0.08 M $NiSO_4.6H_2O$, 0.2 M Na_2SO_4 0.12 M $CoSO_4.7H_2O$, 0.3 M $Na_3C_6H_5O_7.2H_2O$ and 4 g/l of nano-sized Al_2O_3 at time = 20 min., pH = 10, temperature = 25 ˚C and stirring speed = 500 rpm.

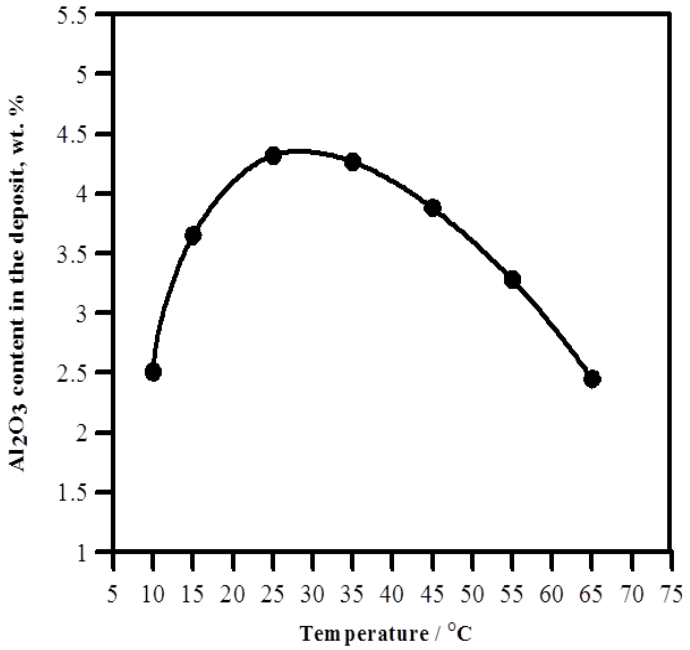

Figure 4. The effect of tub temperature on the composition of Ni-Co / Al_2O_3 composites on steel from a bath with 0.08 M $NiSO_4.6H_2O$, 0.12 M $CoSO_4.7H_2O$, 0.3 M $Na_3C_6H_5O_7.2H_2O$, 0.2 M Na_2SO_4 and 4 g/l of nano-sized Al_2O_3 at time = 20 min., pH = 10, current density = 66.66 mA cm^{-2} and stirring speed = 500 rpm.

The amount of embedded particles in the metallic coatings is based on their amounts in the coating solution. Figure (2) demonstrates the effect of rising nano-sized Al_2O_3 amount in the plating tub on its percentage in the composites. The amount of Al_2O_3 particles in the composite gradually increases with increasing its quantity in the tub and then tends to level off at 5 g/l. The obtained graph is analogous to Langmuir adsorption isotherm [48–51]. This behavior can be explained by adsorption model of Guglielmi [52]. As the quantity of inactive nanoparticles in the solution increases, the number of particles that transfer from the bulk of solution to cathode surface layer increases. Thus, the possibility of striking and adsorption to the electrode surface is enhanced. Consequently, the adsorption speed is accelerated, leading to a higher weight percent of the codeposited Al_2O_3 particles in the metallic matrix. However, the limiting content could be assigned to a steady state of equilibrium. At this state, the number of codepositing particles equals the number attaining the cathode surface [53 & 54].

Current density is the most crucial factors that affecting the codeposition process of inactive particles with metallic matrix from a suspended solution [55]. Figure (3) exhibits the impact of practical current density on the weight percentage of nano-sized Al_2O_3 particles in the deposited Co–Ni alloy. Low current density has no remarked influence on the content of Al_2O_3 in the deposit. Nevertheless, high current densities raise the proportion of Al_2O_3 in the deposit. At low current density and due to the difference in energy of activation demand for deposition, the freely solvated metal ions need small energy for deposition. Consequently, the free Ni^{2+} and Co^{2+} ions will be deposited preferentially on the steel cathode at the expense of Al_2O_3 inert particles. On increasing the current density, the energy difference becomes little important as there is sufficient energy to intensify the

diffusion and convection rates of the particles. This increases both the co-deposition of metallic ions and the unreactive particles [56].

The impact of bath temperature on the amount of nanosized Al_2O_3 particles in Ni–Co coating is shown in Fig. (4). Rising the tub temperature from 10 to 65 °C causes a two-fold effect on deposition of Al_2O_3 particles. As the temperature rises, the kinetic activity of the particles increases, which is helpful for the codeposition of Al_2O_3 particles. In addition, on increasing temperature, the mass transfer of metallic ions is markedly increases by diffusion, convection and migration. This leads to an increase of both kinetic energy and deposition rate. According to Langmuir, the adsorption of adsorbate (inactive particles) diminishes with temperature. This minimizes the chance for Al_2O_3 particles to be instilled in the coat and therefore reduces its percent in the composite [57].

3.3. Morphology and microstructure of composites

The morphological study was investigated to relate characteristics of the composites to electrochemical response during the electrodeposition process. SEM was used for the analysis of composites, obtained under varied experimental conditions. Generally, electrodeposited Ni–Co alloy composites containing Al_2O_3 nanoparticles are orderly, smooth, compact and acquire a dull gray color. The coat brightness increases as the Al_2O_3 proportion increases in the coating. But on the contrary, the darkness of the composites increases with current density.

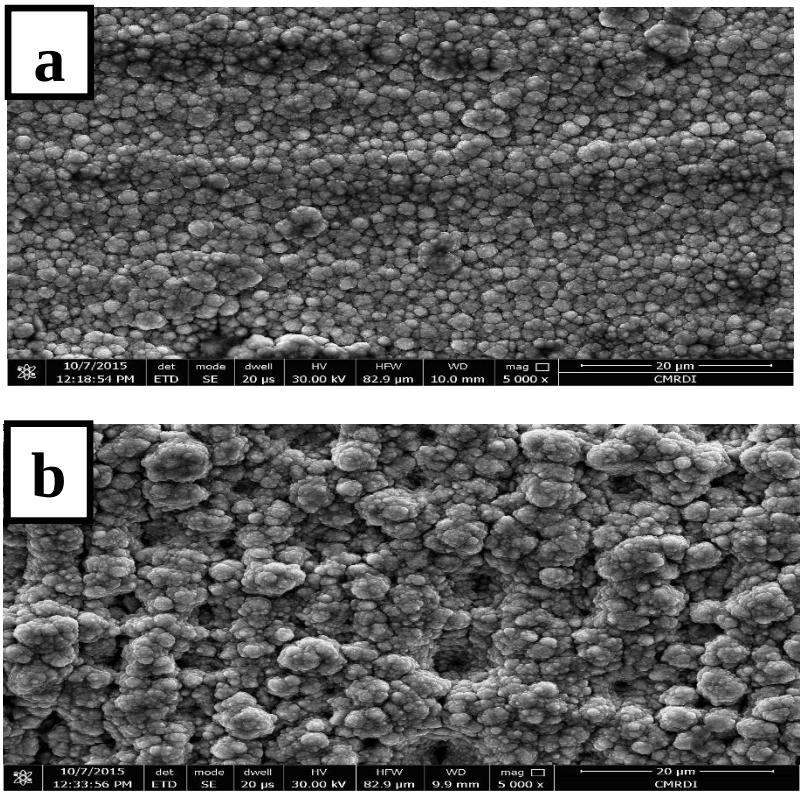

Figure 5. Scanning electron photographs of electrodeposited Ni-Co alloy with: (a) 2.52 and (b) 4.29 wt. % of nano-sized Al_2O_3, obtained from baths with 0.08 M $NiSO_4.6H_2O$, 0.12 M $CoSO_4.7H_2O$, 0.3 M $Na_3C_6H_5O_7.2H_2O$ and 0.2 M Na_2SO_4 at current density = 55.55 mA cm^{-2}, pH = 10, time = 20 min., temp. = 25 °C, stirring speed = 500 rpm.

Figure (5) illustrates the influence of nano-sized Al_2O_3 content in the plating tub on the appearance of electrodeposited Ni–Co composites. The addition of 1 g/l Al_2O_3 particles to the coating tub changes the morphology of the deposit from irregular and dendritic shapes into regular and dense form with small size, Fig. (5a). Further addition of Al_2O_3 changes the morphology of electrodeposited composites to compact agglomerates. Composites contain some pores due to hydrogen evolution. The decrease in size of Ni–Co matrix could be ascribed to the addition of inactive particles to the plating coating tub. During growing of electrodeposited layer, there is a competition between crystal growth and nucleation mechanisms. The unreactive particles adsorbed on a growing lattice and thus, inhibit its growing. This enables more nucleation sites, resulting in small size crystals [58 & 59].

The phase and microstructure of electrodeposited Ni–Co / nano Al_2O_3 composites were tested using XRD measurements. X- ray patterns evidenced that the total composites are crystallized, Fig. 6. The peaks are acute and good – characterized, indicating good crystallization. The structure of the electrodeposited Ni–Co / nano Al_2O_3 composites is a solid solution. It has a face centered cubic (FCC) structure. The electrodeposited alloys showing three – well defined diffraction peaks, (111), (200) and (220), respectively [58 & 59].

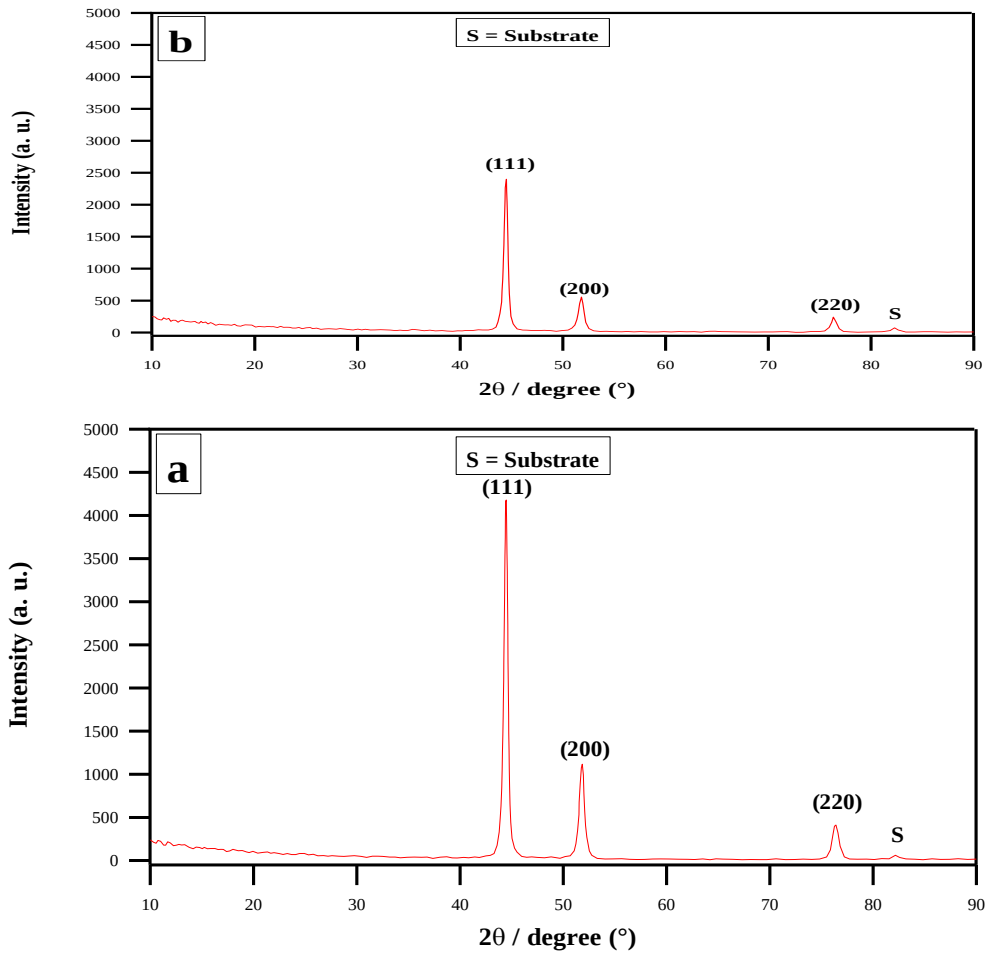

Figure 6. X-ray diffraction of electrodeposited Ni-Co alloy with: (a) 2.52 and (b) 4.29 wt. % of nano-sized Al_2O_3, obtained from baths with 0.08 M $NiSO_4$. $6H_2O$, 0.12 M $CoSO_4$. $7H_2O$, 0.3 M $Na_3C_6H_5O_7$. $2H_2O$ and 0.2 M Na_2SO_4 at current density = 55.55 mA cm^{-2}, pH = 10, time = 20 min., temp. = 25 °C, stirring speed = 500 rpm.

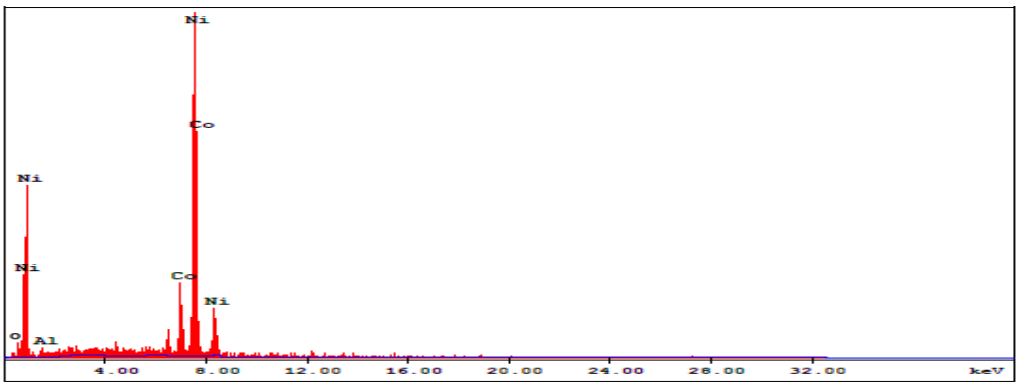

Figure 7. EDX analysis patterns of electrodeposited Ni-Co alloy with: 4.29 wt. % of nano-sized Al_2O_3, obtained from baths with 0.08 M $NiSO_4.6H_2O$, 0.12 M $CoSO_4.7H_2O$, 0.3 M $Na_3C_6H_5O_7.2H_2O$ and 0.2 M Na_2SO_4 at current density = 55.55 mA cm^{-2}, pH = 10, time = 20 min., temp. = 25 ˚C, stirring speed = 500 rpm.

The plane (111) is a predominant one. There are no peaks for Al_2O_3 particles because their proportions in the coating are less than 5 %. EDX analysis confirmed the presence of Al_2O_3, Fig. (7).

3.4. Coating thickness

The coat thickness mainly depends on the imposed current density, the deposition time. Additionally, the amount of dispersed particles in the electrolyte has a noticeable effect on the thickness of the coating [60]. The variation of thickness of electrodeposited Ni–Co / nano Al_2O_3 composites coating with the quantity of incorporated nano Al_2O_3 in the deposit is shown in Table 1. Thickness of Ni–Co / nano Al_2O_3 composite linearly decreases with increasing the percent of Al_2O_3 in the deposit. The reinforced Al_2O_3 particles in the composites behave as barriers which retard the growing of grain. Also, they provide many nucleation positions for the growing of new grains and thence, thinner composites are obtained [61]. The presence of a diffraction apex for steel substrate in XRD patterns confirmed this result.

Table 1. Variation of thickness of composites with Al_2O_3 %

***Al_2O_3 content in composites* (wt. %)**	***Thickness* (µm)**
0	10.9
1.1	9.1
2.5	7.5
3.1	7.1
3.9	6.6
4.3	6.4

3.5. Microhardness

Hardness is considered as important property that characterizes the material because ample practical applications mainly depend on the hardness. Table 2 reveals that there is a detectable elevation in microhardness of Ni–Co / nano Al_2O_3 composite as the percentage of Al_2O_3 increases in the composite.

Table 2. Variation of hardness of composites with Al_2O_3 %

Al_2O_3 content in composites (wt. %))	Hardness (Hv)
0	145
1.1	199
2.5	248
3.1	261
3.9	283
4.3	330

The presence of inactive particles in metal matrix disorders the regular crystalline structure and turns it into a fine crystal structure. The existence of inert particles in the coating influences two competitive processes: formation of metal nuclei and growth of crystals. The addition of particles facilitates greater nucleation sites available for metal ions. This causes higher nucleation rate but low growth rate as it reduces the growing of crystal grains. Accordingly, more uniform surface with a microcrystalline grain is obtained and consequently the microhardness increases.

Furthermore, a section of microhardness improvement in the Ni–Co composite containing Al_2O_3 particles is attributed to the greater microhardness of the Ni–Co alloy, due to formation of substitution type - solid solution [10]. The presence of the latter improves the microhardness of the composites via solid solution hardening mechanism [62].

3.6. Corrosion resistance studies

3.6.1. Potentiodynamic polarization measurements

Anodic and cathodic polarization curves for Ni – Co / nano Al_2O_3 composite in 3.5 % salt water are exhibited in Fig.8. As the % of Al_2O_3 nano – particles increases in the coatings, the rate of corrosion decreases. The values of corrosion potentials, the corrosion current density and other electrochemical parameters were calculated and given in Table 3. The data show that the corrosion current density diminishes with increasing the embedded of Al_2O_3 in the composite.

Table 3. Electrochemical parameters of Ni-Co / nano-Al_2O_3 composites

Sample	βa ($mVdec^{-1}$)	-βc ($mVdec^{-1}$)	I_{corr} ($\mu A\ cm^{-2}$)	R_p (Ω)	-E_{corr} (mV/SCE)	*CR* (mpy)
Ni-Co / 0 wt. % Al_2O_3	237	82	28	933	792	3.7×10^{-4}
Ni-Co / 3.3 wt. % Al_2O_3	226	60	20	1041	761	2.6×10^{-4}
Ni-Co / 3.9 wt. % Al_2O_3	90	10	1.4	2816	722	1.8×10^{-5}
Ni-Co / 4.3 wt. % Al_2O_3	171	347	0.8	62821	562	1.1×10^{-5}

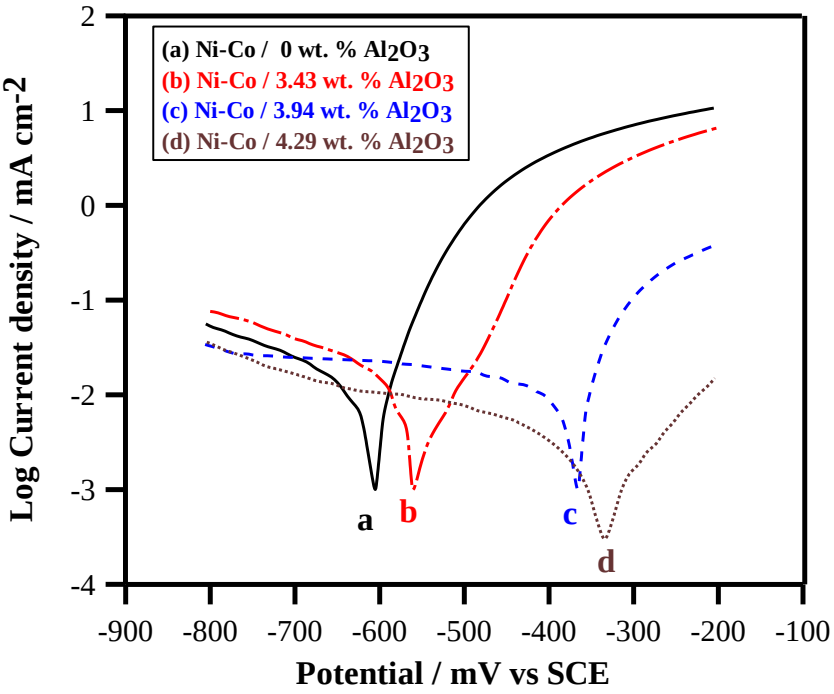

Figure 8. Potentiodynamic polarization for Ni-Co / nano Al_2O_3 composites in 3.5 % salt water at scan rate of 1 mVs^{-1}.

The little rate of corrosion of Ni–Co / nano Al_2O_3 composite could be attributed to contribution of high positive potential Al_2O_3 nanoparticles in the composites. Also the formation of more homogenous structure with small grains reduces the corrosion rate. This may exhibit a high activation barrier, which prevents anodic dissolution. The sum of cathodic and anodic Tafel slopes, βc and βa, does not attain unity because both the anodic and cathodic curves asymmetrical about E_{corr} [63].

3.6.2. Electrochemical impedance spectroscopy studies

Impedance studies for Ni–Co / nano-Al_2O_3 composites in 3.5 wt. % salt water at their OCPs are shown in Fig 9. The compensating circuit that illustrated in Fig. 10 is used to simulate the metal / solution interface, in addition to analyze the Nyquist plots. It composes of a constant phase element (CPE) that is connected in parallel way to the charge transfer resistance (R_{ct}). Both adjoin in series

with the solution resistance (R_s). The constant phase element like a capacitor, but the phase angle does not attain 90°.This is commonly utilized to explicate the inhomogeneity of the system.

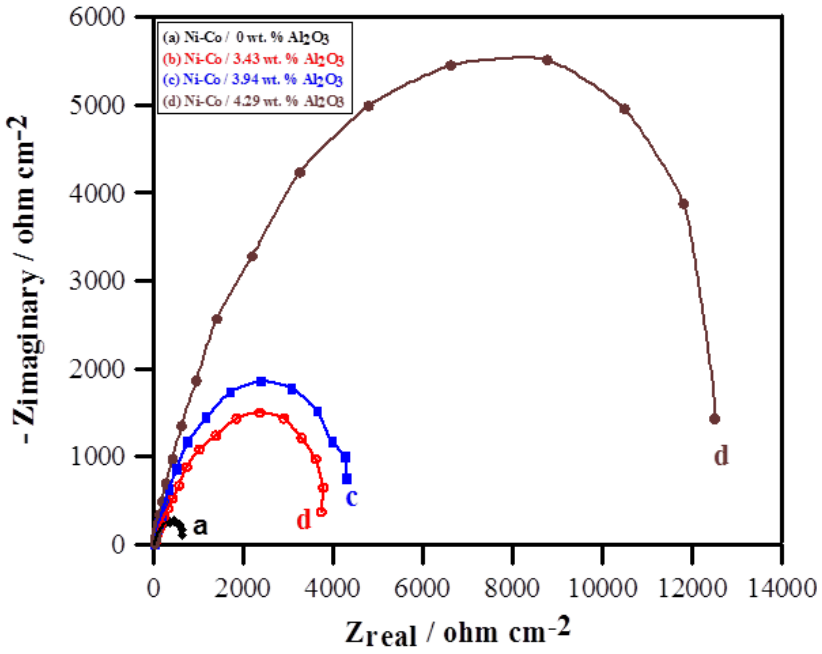

Figure 9. Plots of Nyquist for Ni-Co / nano Al_2O_3 composites in 3.5 % salt water.

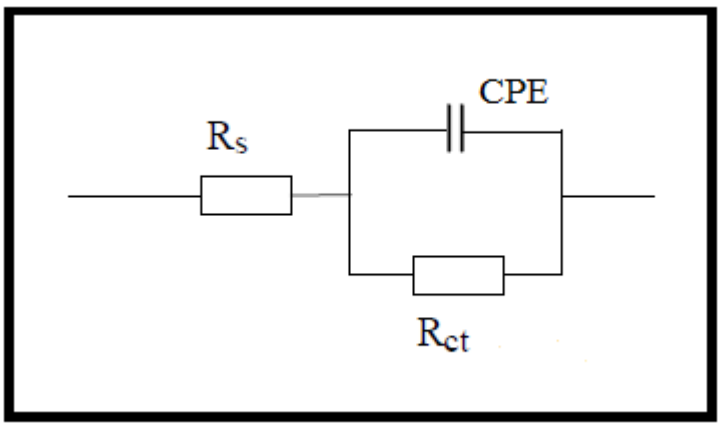

Figure 10. Electrical circuit utilized to fit the practical data of EIS plots.

R_s, R_{ct} & CPE values are listed in Table 4. Nyquist plots obtained for Ni–Co / nano-Al_2O_3 composites exhibited depressed semicircles that differ in width. The width of semicircle reflects the corrosion resistance of the composite. As the semicircle diameter increases, the corrosion resistance increases. The corrosion resistance of the composites increases as the percentage of Al_2O_3 nano – particles increases. The high values of R_{ct} obtained in the present work imply a good corrosion

protective ability for Ni–Co / nano-Al_2O_3 composites. These results are in good agreement with the results of potentiodynamic polarization measurements.

The (CPE) values were evaluated using Brug and others [64] equation. Its value related to the porosity of the coating. The low (CPE) values indicate that the Ni–Co / nano-Al_2O_3 composites are less porous in nature.

Table 4. Electrochemical impedance analysis data for Ni-Co / nano-Al_2O_3 composites in 3.5 % salt water.

Sample	R_s **(Ω cm^{-2})**	R_{ct} **(Ω cm^{-2})**	***CPE*** **(μF cm^{-2})**
Ni-Co / 0 wt. % Al_2O_3	36	600	3710
Ni-Co / 3.3 wt. % Al_2O_3	99	3530	343
Ni-Co / 3.9 wt. % Al_2O_3	138	4160	311
Ni-Co / 4.3 wt. % Al_2O_3	189	11150	183

4. CONCLUSIONS

Application of Ni–Co / nano - Al_2O_3 composite onto low carbon steel cathode was successfully established using electrodeposition technique. Ni–Co / Al_2O_3 nano composites can be prepared by incorporating Al_2O_3 nano-particles to the Ni–Co plating tub. EDX spectroscopy confirmed the existence of nano-scale Al_2O_3 in composites, which increases with increasing its concentration of Al_2O_3 in the plating tub, current density and decreasing temperature. The thickness of Ni–Co / nano - Al_2O_3 coating decreases with increasing the percentage of nano-scale Al_2O_3 in the coating, however the microhardness of the coating increases. Different electrochemical measurements evidenced that Ni–Co / nano - Al_2O_3 composite coatings possess acceptable corrosion resistance in 3.5 % salt water.

ACKNOWLEDGMENT
Authors acknowledge Department of Chemistry, Faculty of Science, Suez Canal University, Central Metallurgical Research & Development Institute, CMRDI, General Organization for Exports and Imports Control (GOEIC), Royal International Inspection Laboratories (RIIL), Department of Chemistry of Sharourah's Faculty of Science and Art, Najran University, for the support for full insight comments.

References

1. M.A. Farrokhzad, G.C. Saha and T.I. Khan, *Surf. Coat. Technol.,* 235 (2013) 75.
2. B. Bakhit, A. Akbari, F. Nasirpouri and M.G. Hosseini, *Appl. Surf. Sci.,* 307 (2014) 351.
3. L. Shi, C. Sun, P. Gao, F. Zhou and W. Liu, *Appl. Surf. Sci.,* 252 (2006) 3591.
4. F. Kılıç, H. Gül, S. Aslan, A. Alp and H. Akbulut, *Colloids and Surfaces A: Physicochem. Eng. Asp.,* 419 (2013) 53.

5. S. Kasturibai and G.P. Kalaignan, *Mater. Chem. Phys.,* 147 (2014) 1042.
6. M. Alizadeh, M. Mirak, E. Salahinejad, M. Ghaffari, R. Amini and A. Roosta, J. *Alloys Compd*., 611 (2014) 161.
7. O. Sancakoglu, O. Culha, M. Toparli, B. Agaday and E. Celik, *Mater. Des.,* 32 (2011) 4054.
8. M. Karbasi, N. Yazdian, and A. Vahidian, *Surf. Coat. Technol.,* 207 (2012) 587.
9. C.T. Low, R.G. Wills and F.C. Walsh, *Surf. Coat. Technol.,* 201 (2006) 371.
10. B. Bakhit and A. Akbari, *J. Alloys Compd.,* 560 (2013) 92.
11. P. Baghery, M. Farzam, A.B. Mousavi and M. Hosseini, *Surf. Coat. Technol.,* 204 (2010) 3804.
12. G.N. Ramesh and S. Jayakrishnan, *Surf. Coat. Technol.,* 206 (2012) 2330.
13. S.M. Lari, A. Amadeh, M.H. Sohi and S.M. Hadavi, *Mater. Sci. Eng A,* 559 (2013) 583.
14. V. Zarghami and M. Ghorbani, *J. Alloys Compd.,* 598 (2014) 236.
15. G.G. Hyung, K. Tripathi, T.H. Kim and S.W. Lee, *J. Mater. Sci. Technol.,* 30 (8) (2014) 796.
16. M. Franco, W. Sha, S. Malinov and R. Rajendran, *Surf. Coat. Technol.,* 235 (2013) 755.
17. S. Mohajeri, A. Dolati and S. Rezagholibeiki, *Mater. Chem. Phys.,* 129 (2011) 746.
18. Q. Feng, T. Li, H. Yue, K. Qi, F. Bai and J. Jin, *Appl. Surf. Sci.,* 254 (2008) 2262.
19. H. Gül, F. Kılıc, M. Uysal, S. Aslan, A. Alp and H. Akbulut, *Appl. Surf. Sci.,* 258 (10) (2012) 4260.
20. L.R. Kanyane, K. Gandazha, O.S. Fayomi and A.P. Popoola, *Procedia Manuf.,* 35 (2019) 814.

21. T. Niu, W.W. Chen, H.W. Cheng and L. Wang, *Trans. Nonferrous Met. Soc. China,* 27 (2017) 2300.
22. B. Bostani, N.P. Ahmadi, S. Yazdani and R. Arghavanian, *Trans. Nonferrous Met. Soc. China,* 28 (1) (2018) 66.
23. T.M. Al-Dhire, H. Zuhailawati and A.S. Anasyida, *Mater. Today: Proc.,* 17 (2019) 664.
24. M. Kartal, I. Buyukbayram, A. Alp, H. Akbulut, *Mater. Today: Proc.,* 4 (2017) 6982.
25. A.A. Aal, Z.I. Zaki and Z.A. Hamid, *Mater. Sci. Eng. A,* 447 (2007) 87.
26. G. Wu, N. Li, D. Zhou and K. Mitsuo, *Surf. Coat. Technol.,* 176 (2004) 157.
27. B.R. Tian and Y.F. Cheng, *Electrochim. Acta,* 53 (2007) 511.
28. B. Szczygieł and M. Kołodziej, *Electrochim. Acta,* 50 (2005) 4188.
29. L.M. Chang, H.F. Guo and M.Z. An, *Mater. Lett.,* 62 (2008) 3313.
30. S. Mahdavi, A.A. Alamdari and M.Z. Meibodi, *Ceram. Int.,* 46 (4) (2020) 5351.
31. M. Alizadeh and A. Cheshmpish, *Appl. Surf. Sci.,* 466 (2019) 433.
32. A. Góral, T. Czeppe and K. Berent, *Surf. Coat. Technol.,* 369 (2019) 95.
33. S.A. Ataie and A. Zakeri, *Surf. Coat. Technol.,* 359 (2019) 206.
34. M. Alizadeh and H. Safaei, *Appl. Surf. Sci.,* 456 (2018)195.
35. C.R. Raghavendra, S. Basavarajappa and I. Sogalad, *Colloids Interface Sci. Commun.,* 27 (2018) 18.
36. A. Góral and S.J. Skrzypek, *Appl. Surf. Sci.,* 456 (2018) 147.
37. A. Góral, *Surf. Coat. Technol.,* 319 (2017) 23.
38. S.W. Jiang, L. Yang, J.N. Pang, H. Lin and Z.Q. Wang, *Surf. Coat. Technol.,* 286 (2016) 197.
39. M.M. Kamel, Z.M. Anwer, I.T. Abdel–Salam and I.S. Ibrahim, *T. I. Met. Finish.,* 88 (4) (2010) 191.
40. K. Vathsala and T.V. Venkatesha, *Appl. Surf. Sci.,* 257 (2011) 8929.
41. A.C. Ciubotariu, L. Benea, M.L. Varsanyi and V. Dragan, *Electrochim. Acta,* 53 (2008) 4557.
42. P.C. Tulio and I.A. Carlos, *J. Appl. Electrochem.,* 39 (2009) 1305.
43. B. Bahadormanesh, A. Dolati and M.R. Ahmadi, *J. Alloys Compd.,* 509 (2011) 9406.
44. X. Cui, W. Wei, H. Liu and W. Chen, *Electrochim. Acta,* 54 (2008) 415.
45. Y.X. Ying, L.K. Ju, P. Xiao and W.F. Hui, *Trans. Nonferrous Met. Soc. China,* 19 (2009) 119.
46. M. Srivastava, V.K. William, A. Jain and K. S. Rajam, *Surf. Coat. Technol.,* 202 (2007) 310.
47. H. Gül, M. Uysal, H. Akbulut and A. Alp, *Surf. Coat. Technol.,* 258 (2014) 1202.
48. Z.A. Hamid and S.M. Elsheikh, *J. Metall. Eng.,* 2 (2) (2013) 71.
49. E.G. Lecina, I.G. Urrutia, J.A. Díez, M. Salvo, F. Smeacetto, G. Gautier, R. Seddon and R. Martin, *Electrochim. Acta,* 54 (2009) 2556.

50. Y.J. Xue, X.Z. Jia, Y.W. Zhou, W. Ma and J.S. Li, *Surf. Coat. Technol.,* 200 (2006) 5677.
51. Z. Yue, Z.G. Gang and Z.H. Jun, *Trans Nonferrous Met. Soc. China,* 20 (2010) 104.
52. N. Guglielmi, *J. Electrochem. Soc.,* 119 (8) (1972) 1009.
53. S. Özkan, G. Hapçı, G. Orhan and K. Kazmanlı, *Surf. Coat. Technol.,* 232 (2013) 734.
54. F. Cai and C. Jiang, *Appl. Surf. Sci.,* 292 (2014) 620.
55. A. Goral, M. Nowak, K. Berent and B. Kania, *J. Alloys Compd.,* 615 (1) (2014) S406.
56. B. Bakhit and A. Akbari, *Surf. Coat. Technol.,* 253 (2014) 76.
57. Y. Yang and Y.F. Cheng, *Surf. Coat. Technol.,* 205 (2011) 3198.
58. M.M. Kamel, J. *Appl. Electrochem.,* 37 (2007) 483.
59. M.M. Kamel, Z.M. Anwer, I.T. Abdel–Salam and I.S. Ibrahim, *Surf. Interface Anal.,* 46 (2014) 442.
60. C. Gheorghies and G. Carac, I.V. Stasi, *J. Optoelectron Adv. M.,* 8 (3) (2006) 1234.
61. T. Borkar and S.P. Harimkar, *Surf. Coat. Technol.,* 205 (2011) 4124.
62. B.M. Praveen and T.V. Venkatesha, *Appl. Surf. Sci.,* 254 (2008) 2418.
63. M.A. Shoeib, M. M. Kamel, S.M. Rashwan and O.M. Hafez, *Surf. Interface Anal.,* 47 (2015) 672.
64. G.J. Brug, A.L. Von, M.S. Rehbach and J.H. Sluyters, *J. Electroanal. Chem.,* 176 (1984) 275.